Quantum Zeno and Anti-Zeno Probes of Noise Correlations in Photon Polarization

Salvatore Virzì⬤, Alessio Avella⬤, Fabrizio Piacentini⬤, and Marco Gramegna⬤
Istituto Nazionale di Ricerca Metrologica, Strada delle Cacce 91, 10135 Torino, Italy

Tomáš Opatrný⬤
Department of Optics, Faculty of Science, Palacký University, 77146 Olomouc, Czech Republic

Abraham G. Kofman⬤
Department of Chemical and Biological Physics, Weizmann Institute of Science, Rehovot 7610001, Israel
and Department of Physics, Shanghai University, 200444 Shanghai, China

Gershon Kurizki
Department of Chemical and Biological Physics, Weizmann Institute of Science, Rehovot 7610001, Israel

Stefano Gherardini⬤ and Filippo Caruso⬤*
Department of Physics and Astronomy and European Laboratory for Non-Linear Spectroscopy (LENS),
University of Florence, via G. Sansone 1, 50019 Sesto Fiorentino, Italy
and Istituto Nazionale di Ottica (CNR-INO), Area Science Park, Basovizza, I-34149 Trieste, Italy

Ivo Pietro Degiovanni⬤ and Marco Genovese⬤
Istituto Nazionale di Ricerca Metrologica, Strada delle Cacce 91, 10135 Torino, Italy
and INFN, sezione di Torino, via P. Giuria 1, 10125 Torino, Italy

We experimentally demonstrate, for the first time, noise diagnostics by repeated quantum measurements, establishing the ability of a single photon subjected to random polarization noise to diagnose non-Markovian temporal correlations of such a noise process. Both the noise spectrum and temporal correlations are diagnosed by probing the photon with frequent (partially) selective polarization measurements. We show that noise with positive temporal correlations corresponds to our single photon undergoing a dynamical regime enabled by the quantum Zeno effect (QZE), whereas noise characterized by negative (anti) correlations corresponds to regimes associated with the anti-Zeno effect (AZE). This is the first step toward a novel noise spectroscopy based on QZE and AZE in single-photon state probing able to extract information on the noise while protecting the probe state, a conceptual paradigm shift with respect to traditional interferometric measurements.

Introduction.—Quantum control [1,2] is a fundamental tool for quantum technologies. In particular, the quantum Zeno effect (QZE) [3–8] and anti-Zeno effect (AZE) [7–11], respectively, denoting the slowdown and speedup of quantum system evolution by its frequent interruptions [12–20], have been recognized (beyond their fundamental significance) as quantum control paradigms [21–26]. Indeed, they allow either protecting [27–29] or steering [30,31] the quantum system state via an interplay between frequent operations (system control) and the coupling of the system to its environment (a bath) [22,32–35].

These paradigms' generality is revealed by the Kofman-Kurizki (KK) universal formula, whereby the overlap of the system-bath coupling spectrum with the system-control spectrum determines the initial-state population decay (relaxation) rate $\gamma(t)$ [9,22,33,34]

$$\gamma(t) = 2\pi \int_{-\infty}^{\infty} d\omega \, G(\omega) F_t(\omega), \qquad (1)$$

being $G(\omega)$ the system-bath coupling spectrum (bath response) and $F_t(\omega)$ the system-control spectrum evaluated within the time interval $[0, t]$. According to Eq. (1), QZE (AZE) corresponds to the suppression (enhancement) of the bath-induced decay $\gamma(t)$ by the reduction (increase) of the overlap between $F_t(\omega)$ and $G(\omega)$ [9,22] (see Supplemental Material [36]). This means that the time variation of the system control must be much faster than (for QZE) or as fast as (for AZE) the bath correlation time, resulting in both effects being distinctly non-Markovian. Overall, the only condition on Eq. (1) validity is the system-bath coupling weakness, allowing for a perturbative treatment of the bath effects. The KK formula

has been confirmed in scenarios involving frequent perturbations of open-system evolution, e.g., cold atom dynamics in optical lattices [12,22], light propagation in waveguides and cavities [5,37], and AZE cooling and QZE heating of bath-coupled qubits [38,39]. Moreover, Eq. (1) can be used for designing optimal protection of multiqubit quantum information processing [40].

Here, we study both theoretically and experimentally an alternative purpose of the KK formula, i.e., the diagnostics (characterization) of random processes, alias noise spectroscopy [41]. One may infer the bath-response spectrum $G(\omega)$ upon varying the control spectrum $F_t(\omega)$ and recording the resulting decoherence rate, as in Ref. [42]. This, however, is a time-consuming process. Alternatively, key information on $G(\omega)$ may be gathered by appropriate dynamical control of the system probing the bath [41]. This represents an innovative and powerful tool that we introduce to expand quantum sensing technology. Although the QZE has been previously used for assisting noise sensing [43,44], here we demonstrate its ability to extract information on noise processes, a direction not yet investigated and highly relevant to quantum technologies. More specifically, we present the first demonstration of noise diagnostics by repeated quantum measurements, showing how a single photon undergoing random polarization fluctuations can diagnose non-Markovian noise temporal correlations. Such a technique may be indispensable under extremely faint illumination, when traditional interferometric methods [45] are usually ineffective. To do this, we realize diverse temporally (anti) correlated noises and their measurement-based single-photon probing proposed in Ref. [32]. We show that the noise temporal correlations can be diagnosed when the single photon undergoes frequent polarization measurements, demonstrating that positive (negative) correlations give rise to QZE (AZE). This paves the way to a new generation of QZE- and AZE-based noise spectroscopy protocols in single-particle state probing.

Theoretical model.—A single photon initialized in the horizontally polarized state $|H\rangle$ passes through a sequence of N blocks at time instants $t_1, \ldots, t_N$. In the kth block (Fig. 1, $k = 1, \ldots, N$), the photon polarization is randomly rotated in the x-z plane of the Bloch sphere by the operator $U(\Delta\phi_k)$ realizing a $\hat{\sigma}_y$ Pauli-matrix rotation around the y axis:

$$U(\Delta\phi_k) = e^{-i\hat{\sigma}_y \Delta\phi_k} = I \cos \Delta\phi_k - i\hat{\sigma}_y \sin \Delta\phi_k, \quad (2)$$

being I the two-dimensional identity matrix. Passing through the N blocks, the horizontal ($|H\rangle$) and vertical ($|V\rangle$) polarization states evolve as the degenerate states of a two-level system coupled by intermittent polarization rotations. These rotations are interspersed by an equivalent number of selective measurements; in each block, the photon undergoes a measurement corresponding to
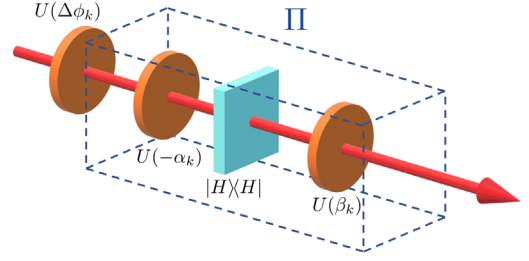

FIG. 1. Scheme of the kth element in a sequence of N blocks determining the quantum state evolution of a photon passing through them. First, the photon undergoes a random polarization rotation $U(\Delta\phi_k)$. Then, the rotation $U(-\alpha_k)$ followed by the projection $|H\rangle\langle H|$ and by a proper counter-rotation $U(\beta_k)$ for suitably chosen α_k, β_k (see Supplemental Material [36]) reproduces the selective measurement Π in Eq. (3) at the kth time instant t_k.

partial or complete absorption of the vertical polarization component (or, equivalently, to partial projection onto the $|H\rangle$ state):

$$\Pi = |H\rangle\langle H| + \theta|V\rangle\langle V| = \theta I + (1 - \theta)|H\rangle\langle H| \quad (3)$$

with $\theta \in [0, 1]$ determining the measurement selective strength. Such an evolution can be realized by an iterative procedure exploiting, in each block, two k-dependent polarization rotations $U(-\alpha_k)$ and $U(\beta_k)$ ($k = 1, \ldots, N$) separated by the projection $|H\rangle\langle H|$. Here, $U(-\alpha_k)$ determines the measurement strength on the state entering the kth block, and $U(\beta_k)$ fixes the polarization of the outgoing photon. By properly choosing the $\{\alpha_k\}$ and $\{\beta_k\}$ coefficients (see Supplemental Material [36]), one can recreate the dynamics induced on the photon polarization by a sequence of N blocks, each performing a random polarization rotation $U(\Delta\phi_k)$ followed by the projector Π in Eq. (3). This is equivalent, in terms of dynamics, to the scheme proposed in Ref. [32].

The kth block output is the (unnormalized) state $|\psi(t_k)\rangle = (\prod_{l=1}^{k}[\Pi U(\Delta\phi_l)])|H\rangle$. Since the sequence $\Delta\phi_1, \ldots, \Delta\phi_N$ is random, because of the external noise process, we are interested in the horizontal polarization survival probability averaged over all possible random sequences

$$\bar{P}_H(t_k) = \overline{|\langle H|\psi(t_k)\rangle|^2}, \quad (4)$$

where the overline denotes the averaging operation.

Consider the case in which the photon undergoes polarization-rotation jumps with identical magnitude, i.e., $|\Delta\phi_k| = \Delta\phi \; \forall \; k = 1, \ldots, N$. We introduce the parameter $\mathcal{C}$ describing the correlation degree between consecutive jumps defined as

$$\overline{\Delta\phi}_{\Delta\phi'} = p\Delta\phi' - (1 - p)\Delta\phi' = \mathcal{C}\Delta\phi', \quad (5)$$

being $\overline{\Delta\phi}_{\Delta\phi'}$ the average polarization rotation jump at the end of the kth block (provided the previous jump was $\Delta\phi'$) and p the correlation probability between subsequent jumps. Thus, jumps are correlated for $\mathcal{C} > 0$ ($p > 0.5$), anticorrelated for $\mathcal{C} < 0$ ($p < 0.5$), and uncorrelated for $\mathcal{C} = 0$ ($p = 0.5$). Although a universal closed-form solution for $\bar{P}_H(t_k)$ is not available, an analytical description of all the cases of interest will follow.

Nonrandom evolution.—In the maximally correlated case $\mathcal{C} = 1$, the time dependence of $\bar{P}_H(t_k)$ is the same as for the nonrandom evolution with identical jumps $\Delta\phi$ or $(-\Delta\phi)$ in each block. In particular, $\forall\, \theta$ one has [32]

$$\bar{P}_H(t_k) = \frac{[\lambda_+^k(\cos\Delta\phi - \lambda_-) + \lambda_-^k(\lambda_+ - \cos\Delta\phi)]^2}{(1+\theta)^2\cos^2\Delta\phi - 4\theta} \quad (6)$$

with $\lambda_\pm \equiv \frac{1}{2}[(1+\theta)\cos\Delta\phi \pm \sqrt{(1+\theta)^2\cos^2\Delta\phi - 4\theta}]$. In the absence of measurements ($\theta = 1$), one gets $\bar{P}_H(t_k) = \cos^2(k\Delta\phi)$ analogous to Rabi oscillations of $\bar{P}_H(t_k)$ as a function of the number of blocks k. For $\theta = 0$, one recovers the selective (projective) measurement case, since each time a photon passes through a block its polarization state is projected onto $|H\rangle$; here we have $\bar{P}_H(t_k) = \cos^{2k}(\Delta\phi)$, insensitive to jump sign fluctuations and hence identical for random and nonrandom evolution, becoming $\bar{P}_H(t_k) = e^{-k(\Delta\phi)^2}$ for small rotation angles ($\Delta\phi \ll 1$). This decay is slower than the period of uninterrupted Rabi oscillations, i.e., QZE occurs. Next, consider nonrandom evolution with $0 < \theta < 1$ corresponding to partially selective measurements [46]. For small rotation angles and sufficient selective strength ($\Delta\phi \ll 1 - \theta$), Eq. (6) reduces to $\bar{P}_H(t_k) = \exp\{-[(\Delta\phi)^2/\tau^2\nu]t_k\}$, with $\nu \equiv [(1-\theta)/(1+\theta)](1/\tau)$ and the N blocks assumed to be equidistant ($t_k = k\tau$, being τ the photon flight time between consecutive blocks). The quantity ν is the (effective) measurement rate, i.e., the reciprocal time during which state selection occurs, scaling as $1/\tau$ and decreasing as θ increases. The decay rate diminishes with ν, highlighting the QZE.

Random evolution.—Consider the case of random noisy modulation of $U(\Delta\phi)$ for (anti) correlated noise ($-1 \le \mathcal{C} < 1$). For $\Delta\phi \ll 1$, one has ($\forall\, \theta$) [32]

$$\bar{P}_H(t_k) = e^{-(\gamma+\Gamma_0)t_k}\left(\cosh(St_k) + \frac{\Gamma_0}{S}\sinh(St_k)\right), \quad (7)$$

where $S \equiv \sqrt{\gamma^2 + \Gamma_0^2}$, $\gamma \equiv [(1+\mathcal{C}\theta)/(1-\mathcal{C}\theta)](\Delta\phi^2/\tau)$ is the polarization decay rate, and $\Gamma_0 \equiv -(\ln\theta/2\tau)$ denotes the time-averaged rate of photons absorbed by the polarizers (see Supplemental Material [36]).

Without measurements ($\theta = 1$), Eq. (7) yields

$$\bar{P}_H(t_k) = \frac{1 + e^{-2\gamma_0 t_k}}{2} \qquad (\gamma_0 \equiv \gamma|_{\theta=1}). \quad (8)$$
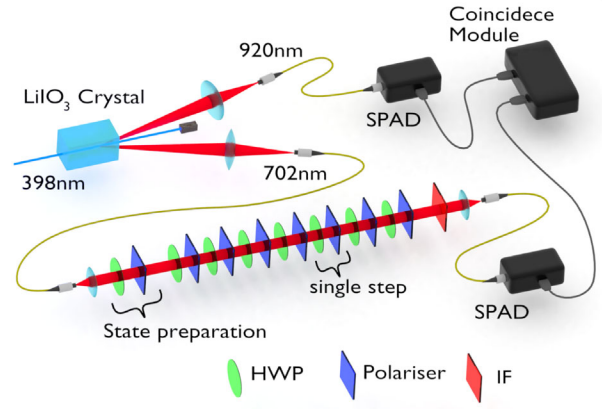

FIG. 2. Heralded single photons at 702 nm generated by type-I parametric down-conversion are fiber coupled and then collimated in a Gaussian beam (2 mm width) over a 2-m-long path. After being prepared in the $|H\rangle$ state by a polarizer, each photon passes through a series of $N = 7$ polarization rotation and measurement stages. When Zeno measurements occur, each stage hosts a half-wave plate (HWP) and a polarizer, while without measurements only a HWP is present (after the Nth stage, a polarizer performs the final projection $|H\rangle\langle H|$). An interference filter (IF, 3 nm FWHM) removes environmental light, then the photons are fiber coupled and detected by a silicon single-photon avalanche diode (SPAD).

Thus, random polarization fluctuations lead to complete unpolarization, i.e., $\bar{P}_H(t) \to 1/2$ for $t \to \infty$.

For weakly selective measurements ($\theta \to 1$), in the limit $\Gamma_0 \ll \gamma$ Eq. (7) becomes

$$\bar{P}_H(t_k) \approx e^{-\gamma t_k}, \quad (9)$$

showing an exponential decay over time of the horizontal polarization probability.

Finally, for projective measurements ($\theta \to 0$), $\bar{P}_H(t_k)$ evolves following Eq. (9), with $\gamma \to \Delta\phi^2/\tau$.

Experimental results.—In our setup (Fig. 2), single photons initialized in the $|H\rangle$ state traverse $N = 7$ stages hosting a half-wave plate (HWP) and a polarizer, reproducing the dynamics of a sequence of $N = 7$ blocks in Fig. 1. For each k, the HWP reproduces the combined effect of the global rotation $U(\alpha_k)U(\Delta\phi_k)U(\beta_{k-1})$, while the polarizer realizes the projector $|H\rangle\langle H|$. Every stage induces a random polarization rotation jump $\pm\Delta\phi$ (selected by a random number generator, with $\Delta\phi = 4°$) and realizes the (partially) selective measurement Π in Eq. (3). Each jump is set to be equal (correlated) to the previous one with probability $p = [(\mathcal{C} + 1)/2]$. At the end of the sequence, only horizontally polarized photons are detected. We have three possible handles on $\bar{P}_H(t_k)$: (i) the parameter θ determining the strength of the measurement Π in Eq. (3), (ii) the correlation coefficient $\mathcal{C}$, and (iii) the polarization jump amplitude $\Delta\phi$. In the experiment we investigated three cases, $\mathcal{C} = -0.6$, 0, and 0.4, while
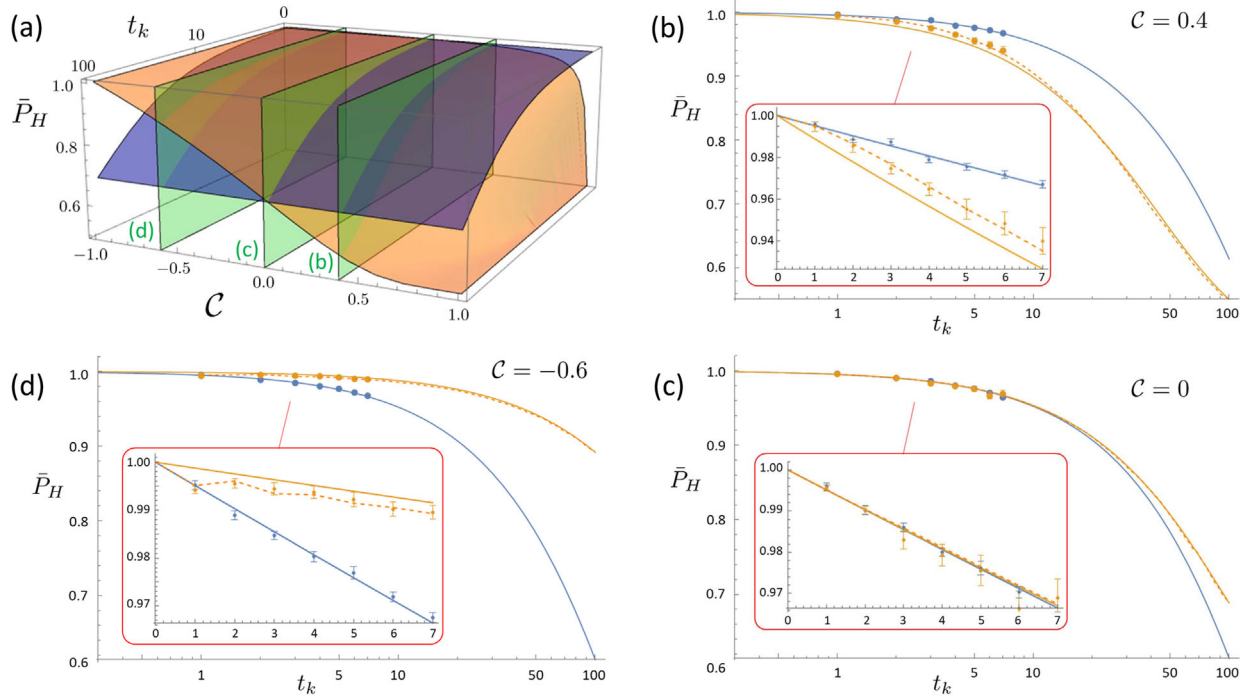
FIG. 3. QZE (AZE) effect as a signature of (anti) correlated noise. (a) Theoretical average probability $\bar{P}_H(t_k)$ for (anti) correlated consecutive jumps of magnitude $\Delta\phi = 4°$ as a function of t_k and the correlation parameter $\mathcal{C}$, in the presence ($\theta = 0$, blue surface) and absence ($\theta = 1$, orange surface) of measurement. The green planes indicate the $\mathcal{C}$ values considered in our experiment, whose results are shown in (b)–(d). There, the experimental data are shown for both $\theta = 1$ (orange) and $\theta = 0$ (blue), with the statistical uncertainties evaluated as the standard deviation of 100 different realizations. The solid curves show the theoretical predictions given by Eqs. (8) and (9), respectively. The dashed orange lines represent, instead, $\bar{P}_H(t_k)$ numerical estimations for $\theta = 1$, as per Eq. (4), obtained by averaging over 100 simulated random sequences of $\pm\Delta\phi$ jumps. The inset plots show, in detail, the experimentally investigated region $t_k \in [0, 7]$.

varying θ and keeping $\Delta\phi = 4°$. For each $\mathcal{C}$ value, we measured the single-photon detection probabilities and standard deviations (uncertainties) of 100 random sequences of $N = 7$ jumps. Figure 3 presents the behavior of $\bar{P}_H(t_k)$ with respect to t_k for $\theta = 0$, corresponding to a projective measurement, and $\theta = 1$, i.e., in the absence of measurement (the measurement strength decreases as θ increases). Figure 4, instead, shows the results obtained for $0 < \theta < 1$, i.e., from the projective limit to the weakly selective one. In the Markovian case $\mathcal{C} = 0$, the measured probability is independent of θ. The novel result is that for $\mathcal{C} > 0$ ($\mathcal{C} < 0$), the QZE (AZE) is revealed, meaning slowdown (speedup) of the decay compared to the uncorrelated case. By varying θ, one can promote or suppress both effects [32,47,48]. In both Figs. 3 and 4, the obtained results (dots) are in good agreement with the theoretical predictions (lines).

Finally, for each noise (anti) correlation regime, we estimated the correlation parameter $\mathcal{C}$ by comparing the $\bar{P}_H$ value at the end of our process with and without Zeno measurements ($\bar{P}_H^{(\theta=0)}$ and $\bar{P}_H^{(\theta=1)}$, respectively). By interpolating the results of numerical simulations based on Eq. (4), we can extract the dependence of $\mathcal{C}$ on the difference $\Delta\bar{P}_H = \bar{P}_H^{(\theta=0)} - \bar{P}_H^{(\theta=1)}$ (Fig. 5). From the experimental $\Delta\bar{P}_H$ values and uncertainties (orange dashed and solid

lines, respectively), we can estimate the corresponding $\mathcal{C}^{(exp)}$ (green dashed line). For each regime investigated, the green solid lines delimit the confidence interval $\mathcal{I}_{\mathcal{C}}$ on $\mathcal{C}^{(exp)}$ obtained propagating the experimental uncertainty on $\Delta\bar{P}_H$ and reported in the inset table together with $\mathcal{C}^{(exp)}$ and the theoretical values $\mathcal{C}^{(th)}$.
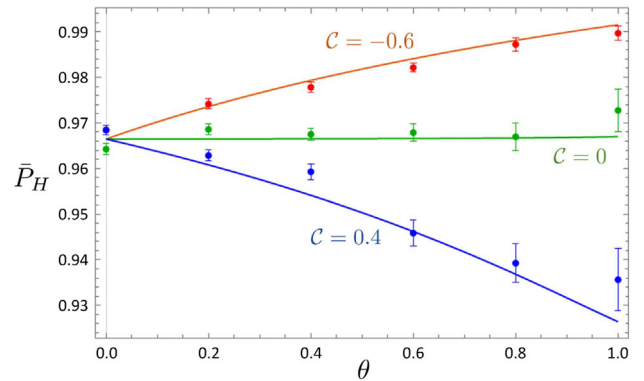

FIG. 4. Average probability $\bar{P}_H(t_7)$ at the end of our protocol as a function of the Π measurement strength θ [Eq. (3)], for the three $\mathcal{C}$ values chosen for our experiment. Lines: theoretical predictions given by Eq. (7) for $\tau = 1$ and $k = 7$. Dots: measured $\bar{P}_H(t_7)$ values. Experimental uncertainties are evaluated as the standard deviation of the 100 different realizations results.
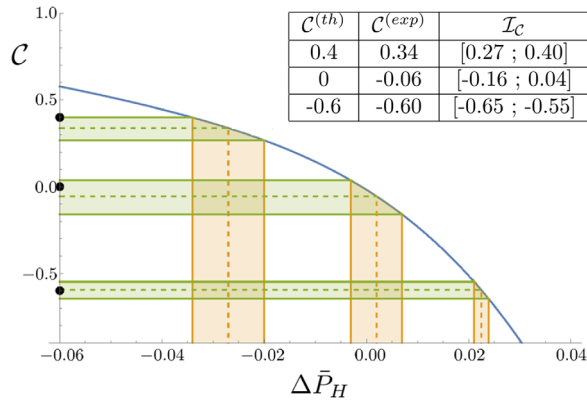
$\mathcal{C}^{(th)}$	$\mathcal{C}^{(exp)}$	$\mathcal{I}_{\mathcal{C}}$
0.4	0.34	[0.27 ; 0.40]
0	-0.06	[-0.16 ; 0.04]
-0.6	-0.60	[-0.65 ; -0.55]

FIG. 5. Estimation of the noise correlation parameter $\mathcal{C}$ from the difference $\Delta \bar{P}_H = \bar{P}_H^{(\theta=0)} - \bar{P}_H^{(\theta=1)}$, being $\bar{P}_H^{(\theta=0)}$ and $\bar{P}_H^{(\theta=1)}$ the average probabilities of detecting a horizontally polarized photon with or without Zeno measurements, respectively. Blue curve: dependence of $\mathcal{C}$ on $\Delta \bar{P}_H$ obtained from numerical simulations based on Eq. (4). Orange dashed and solid lines: experimental $\Delta \bar{P}_H$ values and uncertainties for $\mathcal{C} = -0.6$, $\mathcal{C} = 0$, and $\mathcal{C} = 0.4$ (black dots on the Y axis). Green dashed and solid lines: extracted $\mathcal{C}$ values and associated 1σ confidence intervals (being σ the uncertainty on the measured $\Delta \bar{P}_H$) obtained by propagating the uncertainties on $\Delta \bar{P}_H$. The inset table hosts the theoretical $\mathcal{C}$ values ($\mathcal{C}^{(th)}$), the experimentally obtained ones ($\mathcal{C}^{(exp)}$), and the associated confidence intervals ($\mathcal{I}_{\mathcal{C}}$).

All the estimated values are in good agreement with their theoretical counterparts, certifying the reliability and robustness of our single-photon technique for noise temporal correlations estimation.

Here, we considered linear polarization rotations of equal magnitude around a fixed axis. Yet, our method can be extended to far more general noise classes. To prove this, we performed numerical simulations considering a generic polarization noise model, i.e., polarization jumps with random amplitude along any randomly chosen axis of the Bloch sphere. Our simulations (see Supplemental Material [36]) demonstrate that behavior akin to our proof-of-principle experiment can be observed for very general noise classes, for which our protocol allows estimating qualitatively (and even quantitatively) the correlation parameter $\mathcal{C}$. Such a generalization requires the adaptation of our experimental procedure by inserting further quarter- and half-wave plates to realize generic polarization rotations. The investigation of this scenario, as well as of methods for increasing the number of blocks [49], is demanded to further studies.

Conclusions.—We experimentally investigated the polarization coherence loss for a single photon undergoing stochastic polarization noise and, concurrently, frequent (weak or strong) selective quantum measurements, demonstrating that the polarization decay rate depends on non-Markovian correlations within the noise. The key feature is that (anti) correlated jumps give rise to decay-rate

slowdown (speedup), giving rise to QZE (AZE), fully complying with the KK universal formula for the decay-rate dependence on the overlap between the noise and frequent-measurement spectra [9,22,34]. This demonstration enables the use of photons and other particles as probes of noise correlations. As shown above, a limited number (here, 100) of single-photon polarization coherence loss events in a noisy medium probed by a few (here, $N = 7$) selective measurements can reveal unequivocally the noise correlation characteristics. Characterizing noise, especially in non-Markovian processes [50–52], is crucial for several quantum technologies. To this end, our scheme may be modified by inserting a fluctuating birefringent medium between consecutive measurements [28], thereby allowing the sensing [41] of the polarization noise spectrum associated with a propagating photon.

As an example, among the envisaged applications of the proposed noise sensing method we may contemplate the probing of magnetic field fluctuations, translated into photon polarization fluctuations through the Faraday effect [53–56]. Single-photon probing of such fluctuations may allow for the exploration of vacuum magnetic birefringence [57], parity violation in atoms [58], and weak-magnetic-noise calibration [59]. Further applications conceive disordered media [60] and physiological processes sensing, like polarization microscopy of birefringent cholesterol crystals in human biological (synovial, pleural, and pericardial) fluids to diagnose rheumatoid diseases [61–63] and atherosclerosis [64]. Finally, chirality plays a relevant role in protein biosynthesis, allowing for polarization-based biophysical techniques for protein structure characterization [65,66]; combining these methods with our sensing technique could allow us to study biopolymer synthesis and evolution, investigating correlations among morphological structures during biochemical processes.

To conclude, we established the possibility of probing correlations in photon polarization fluctuations by QZE and AZE observation. Our noise sensing procedure, different from interferometric measurements [45], works even at extremely low illumination levels, allowing its application to highly photosensitive materials and molecules that should absorb (almost) no photon. This paves the way to a new kind of quantum sensing techniques, extracting information on the noise affecting a quantum channel while preserving the probe quantum state.

---

*Corresponding author.
filippo.caruso@unifi.it

[1] H. M. Wiseman and G. J. Milburn, *Quantum Measurement and Control* (Cambridge University Press, Cambridge, England, 2009).

[2] C. Brif, R. Chakrabarti, and H. Rabitz, Control of quantum phenomena: Past, present and future, New J. Phys. **12**, 075008 (2010).

[3] B. Misra and E. C. G. Sudarshan, The Zeno's paradox in quantum theory, J. Math. Phys. (N.Y.) **18**, 756 (1977).

[4] W. M. Itano, D. J. Heinzen, J. J. Bollinger, and D. J. Wineland, Quantum Zeno effect, Phys. Rev. A **41**, 2295 (1990).

[5] A. G. Kofman and G. Kurizki, Quantum Zeno effect on atomic excitation decay in resonators, Phys. Rev. A **54**, R3750 (1996).

[6] D. Home and M. Whitaker, A conceptual analysis of quantum Zeno; paradox, measurement, and experiment, Ann. Phys. (N.Y.) **258**, 237 (1997).

[7] K. Koshino and A. Shimizu, Quantum Zeno effect by general measurements, Phys. Rep. **412**, 191 (2005).

[8] K. Thapliyal, A. Pathak, and J. Peřina, Linear and nonlinear quantum Zeno and anti-Zeno effects in a nonlinear optical coupler, Phys. Rev. A **93**, 022107 (2016).

[9] A. G. Kofman and G. Kurizki, Acceleration of quantum decay processes by frequent observations, Nature (London) **405**, 546 (2000).

[10] P. Facchi, H. Nakazato, and S. Pascazio, From the Quantum Zeno to the Inverse Quantum Zeno Effect, Phys. Rev. Lett. **86**, 2699 (2001).

[11] M. Yamaguchi, T. Asano, and S. Noda, Photon emission by nanocavity-enhanced quantum anti-Zeno effect in solid-state cavity quantum-electrodynamics, Opt. Express **16**, 18067 (2008).

[12] M. C. Fischer, B. Gutiérrez-Medina, and M. G. Raizen, Observation of the Quantum Zeno and Anti-Zeno Effects in an Unstable System, Phys. Rev. Lett. **87**, 040402 (2001).

[13] P. Facchi and S. Pascazio, Quantum Zeno Subspaces, Phys. Rev. Lett. **89**, 080401 (2002).

[14] F. Schäfer, I. Herrera, S. Cherukattil, C. Lovecchio, F. S. Cataliotti, F. Caruso, and A. Smerzi, Experimental realization of quantum Zeno dynamics, Nat. Commun. **5**, 3194 (2014).

[15] A. Signoles, A. Facon, D. Grosso, I. Dotsenko, S. Haroche, J.-M. Raimond, M. Brune, and S. Gleyzes, Confined quantum Zeno dynamics of a watched atomic arrow, Nat. Phys. **10**, 715 (2014).

[16] S. Gherardini, S. Gupta, F. S. Cataliotti, A. Smerzi, F. Caruso, and S. Ruffo, Stochastic quantum Zeno by large deviation theory, New J. Phys. **18**, 013048 (2016).

[17] M. M. Müller, S. Gherardini, and F. Caruso, Stochastic quantum Zeno-based detection of noise correlations, Sci. Rep. **6**, 38650 (2016).

[18] P. Facchi and S. Pascazio, Quantum Zeno dynamics: Mathematical and physical aspects, J. Phys. A **41**, 493001 (2008).

[19] P. G. Kwiat, A. G. White, J. R. Mitchell, O. Nairz, G. Weihs, H. Weinfurter, and A. Zeilinger, High-Efficiency Quantum Interrogation Measurements via the Quantum Zeno Effect, Phys. Rev. Lett. **83**, 4725 (1999).

[20] H. Zheng, S. Y. Zhu, and M. S. Zubairy, Quantum Zeno and Anti-Zeno Effects: Without the Rotating-Wave Approximation, Phys. Rev. Lett. **101**, 200404 (2008).

[21] M. M. Müller, S. Gherardini, and F. Caruso, Quantum Zeno dynamics through stochastic protocols, Ann. Phys. (Amsterdam) **529**, 1600206 (2017).

[22] A. G. Kofman and G. Kurizki, Universal Dynamical Control of Quantum Mechanical Decay: Modulation of the Coupling to the Continuum, Phys. Rev. Lett. **87**, 270405 (2001).

[23] L. Zhou, S. Yang, Y.-x. Liu, C. P. Sun, and F. Nori, Quantum Zeno switch for single-photon coherent transport, Phys. Rev. A **80**, 062109 (2009).

[24] S. Hacohen-Gourgy, L. P. García-Pintos, L. S. Martin, J. Dressel, and I. Siddiqi, Incoherent Qubit Control Using the Quantum Zeno Effect, Phys. Rev. Lett. **120**, 020505 (2018).

[25] A. Pechen, N. Il'in, F. Shuang, and H. Rabitz, Quantum control by von Neumann measurements, Phys. Rev. A **74**, 052102 (2006).

[26] J. J. W. H. Sørensen, M. Dalgaard, A. H. Kiilerich, K. Mølmer, and J. F. Sherson, Quantum control with measurements and quantum Zeno dynamics, Phys. Rev. A **98**, 062317 (2018).

[27] S. Maniscalco, F. Francica, R. L. Zaffino, N. Lo Gullo, and F. Plastina, Protecting Entanglement via the Quantum Zeno Effect, Phys. Rev. Lett. **100**, 090503 (2008).

[28] F. Piacentini, A. Avella, E. Rebufello, R. Lussana, F. Villa, A. Tosi, M. Gramegna, G. Brida, E. Cohen, L. Vaidman, I. P. Degiovanni, and M. Genovese, Determining the quantum expectation value by measuring a single photon, Nat. Phys. **13**, 1191 (2017).

[29] G. A. Paz-Silva, A. T. Rezakhani, J. M. Dominy, and D. A. Lidar, Zeno Effect for Quantum Computation and Control, Phys. Rev. Lett. **108**, 080501 (2012).

[30] X.-B. Wang, J. Q. You, and F. Nori, Quantum entanglement via two-qubit quantum Zeno dynamics, Phys. Rev. A **77**, 062339 (2008).

[31] G. Barontini, L. Hohmann, F. Haas, J. Estve, and J. Reichel, Deterministic generation of multiparticle entanglement by quantum Zeno dynamics, Science **349**, 1317 (2015).

[32] A. G. Kofman, G. Kurizki, and T. Opatrný, Zeno and anti-Zeno effects for photon polarization dephasing, Phys. Rev. A **63**, 042108 (2001).

[33] A. G. Kofman and G. Kurizki, Unified Theory of Dynamically Suppressed Qubit Decoherence in Thermal Baths, Phys. Rev. Lett. **93**, 130406 (2004).

[34] J. Clausen, G. Bensky, and G. Kurizki, Bath-Optimized Minimal-Energy Protection of Quantum Operations from Decoherence, Phys. Rev. Lett. **104**, 040401 (2010).

[35] P. M. Harrington, J. T. Monroe, and K. W. Murch, Quantum Zeno Effects from Measurement Controlled Qubit-Bath Interactions, Phys. Rev. Lett. **118**, 240401 (2017).

[36] See Supplemental Material at http://link.aps.org/supplemental/10.1103/PhysRevLett.129.030401 for details on the theoretical model and on the iterative procedure present in the experiment, and for a numerical study on the robustness of our noise sensing technique with respect to general noise processes.

[37] P. Biagioni, G. Della Valle, M. Ornigotti, M. Finazzi, L. Duò, P. Laporta, and S. Longhi, Experimental demonstration of the optical Zeno effect by scanning tunneling optical microscopy, Opt. Express **16**, 3762 (2008).

[38] N. Erez, G. Gordon, M. Nest, and G. Kurizki, Thermodynamic control by frequent quantum measurements, Nature (London) **452**, 724 (2008).

[39] G. A. Álvarez, D. D. Bhaktavatsala Rao, L. Frydman, and G. Kurizki, Zeno and Anti-Zeno Polarization Control of Spin Ensembles by Induced Dephasing, Phys. Rev. Lett. **105**, 160401 (2010).

[40] G. Gordon and G. Kurizki, Universal dephasing control during quantum computation, Phys. Rev. A **76**, 042310 (2007).

[41] A. Zwick, G. A. Álvarez, and G. Kurizki, Maximizing Information on the Environment by Dynamically Controlled Qubit Probes, Phys. Rev. Applied **5**, 014007 (2016).

[42] C. O. Bretschneider, G. A. Álvarez, G. Kurizki, and L. Frydman, Controlling Spin-Spin Network Dynamics by Repeated Projective Measurements, Phys. Rev. Lett. **108**, 140403 (2012).

[43] H.-V. Do, C. Lovecchio, I. Mastroserio, N. Fabbri, F. S. Cataliotti, S. Gherardini, M. M. Müller, N. Dalla Pozza, and F. Caruso, Experimental proof of quantum Zeno-assisted noise sensing, New J. Phys. **21**, 113056 (2019).

[44] M. M. Müller, S. Gherardini, N. Dalla Pozza, and F. Caruso, Noise sensing via stochastic quantum Zeno, Phys. Lett. A **384**, 126244 (2020).

[45] M. O. Scully and M. S. Zubairy, *Quantum Optics* (Cambridge University Press, Cambridge, England, 1997).

[46] B. Tamir and E. Cohen, Introduction to weak measurements and weak values, Quanta **2**, 7 (2013).

[47] G. J. Milburn, Quantum Zeno effect and motional narrowing in a two-level system, J. Opt. Soc. Am. B **5**, 1317 (1988).

[48] A. Peres and A. Ron, Incomplete "collapse" and partial quantum Zeno effect, Phys. Rev. A **42**, 5720 (1990).

[49] B. Sephton, A. Dudley, G. Ruffato, F. Romanato, L. Marrucci, M. Padgett, S. Goyal, F. Roux, T. Konrad, and A. Forbes, A versatile quantum walk resonator with bright classical light, PLoS One **14**, e0214891 (2019).

[50] C. Benedetti, M. G. A. Paris, and S. Maniscalco, Non-Markovianity of colored noisy channels, Phys. Rev. A **89**, 012114 (2014).

[51] R. B. Wu, T. F. Li, A. G. Kofman, J. Zhang, Y.-X. Liu, Y. A. Pashkin, J.-S. Tsai, and F. Nori, Spectral analysis and identification of noises in quantum systems, Phys. Rev. A **87**, 022324 (2013).

[52] S. Banerjee, J. Naikoo, and R. Srikanth, Distinguishing environment-induced non-Markovianity from subsystem dynamics, Int. J. Quantum. Inform. **18**, 2050042 (2020).

[53] D. Goldring, Z. Zalevsky, G. Shabtay, D. Abraham, and D. Mendlovic, Magneto-optic-based devices for polarization control, J. Opt. A **6**, 98 (2004).

[54] X. S. Yao, L. Yan, and Y. Shi, Highly repeatable all-solid-state polarization-state generator, Opt. Lett. **30**, 1324 (2005).

[55] L. Chen and W. She, Arbitrary-to-linear or linear-to-arbitrary polarization controller based on Faraday and Pockels effects in a single BGO crystal, Opt. Express **15**, 15589 (2007).

[56] T. Saitoh and S. Kinugawa, Magnetic field rotating-type Faraday polarization controller, IEEE Photonics Technol. Lett. **15**, 1404 (2003).

[57] M. J. D. Macpherson, K. P. Zetie, R. B. Warrington, D. N. Stacey, and J. P. Hoare, Precise Measurement of Parity Nonconserving Optical Rotation at 876 nm in Atomic Bismuth, Phys. Rev. Lett. **67**, 2784 (1991).

[58] A. H. Gevorgyan, M. Z. Harutyunyan, S. A. Mkhitaryan, E. A. Santrosyan, and G. A. Vardanyan, A polarization amplifier and stabilizer based on Fabri-Perot resonator filled with chiral photonic crystal, Optik (Stuttgart) **121**, 39 (2010).

[59] D. M. Meekhof, P. Vetter, P. K. Majumder, S. K. Lamoreaux, and E. N. Fortson, High-Precision Measurement of Parity Nonconserving Optical Rotation in Atomic Lead, Phys. Rev. Lett. **71**, 3442 (1993).

[60] M. Leonetti, L. Pattelli, S. De Panfilis, D. S. Wiersma, and G. Ruocco, Spatial coherence of light inside three-dimensional media, Nat. Commun. **12**, 4199 (2021).

[61] M. M. Zakharova, V. A. Nasonova, A. F. Konstantinova, V. S. Chudakov, and R. V. Gaĭnutdinov, An investigation of the optical properties of cholesterol crystals in human synovial fluid, Crystallogr. Rep. (Transl. Kristallografiya) **54**, 509 (2009).

[62] M. W. Ropes and W. Bauer, Synovial fluid changes in joint disease, J. Bone Jt. Surg. **36** (1954).

[63] W. H. R. Nye, R. Terry, and D. L. Rosenbaum, Two forms of crystalline lipid in "cholesterol" effusions, American Journal of Clinical Pathology **49**, 718 (1968).

[64] M. Kashiwagi, L. Liu, K. K. Chu, C.-H. Sun, A. Tanaka, J. A. Gardecki, and G. J. Tearney, Feasibility of the assessment of cholesterol crystals in human macrophages using micro optical coherence tomography, PLoS One **9**, 1 (2014).

[65] L. Whitmore and B. A. Wallace, Protein secondary structure analyses from circular dichroism spectroscopy: Methods and reference databases, Biopolymers **89**, 392 (2008).

[66] A. J. Miles and B. A. Wallace, Circular dichroism spectroscopy of membrane proteins, Chem. Soc. Rev. **45**, 4859 (2016).